ISSN 1063-7788, Physics of Atomic Nuclei, 2015, Vol. 78, No. 2, pp. 220–229. © Pleiades Publishing, Ltd., 2015.
Original Russian Text © S.S. Belyshev, L.Z. Dzhilavyan, B.S. Ishkhanov, I.M. Kapitonov, A.A. Kuznetsov, V.N. Orlin, K.A. Stopani, 2015, published in Yadernaya Fizika, 2015, Vol. 78, Nos. 3-4, pp. 246–255.

NUCLEI
Theory

Photonuclear Reactions on Titanium Isotopes

S. S. Belyshev[1)], L. Z. Dzhilavyan[2)], B. S. Ishkhanov[1),3)], I. M. Kapitonov[1)], A. A. Kuznetsov[3)*], V. N. Orlin[3)], and K. A. Stopani[3)]

Received July 14, 2014; in final form, September 9, 2014

Abstract—The photodisintegration of titanium isotopes in the giant-dipole-resonance energy region is studied by the photon-activation method. Bremsstrahlung photons whose spectrum has the endpoint energy of 55 MeV is used. The yields and integrated cross sections are determined for photoproton reactions on the titanium isotopes ^{47,48,49,50}Ti. The respective experimental results are compared with their counterparts calculated on the basis of the TALYS code and a combined photonucleon-reaction model. The TALYS code disregards the isospin structure of the giant dipole resonance and is therefore unable to describe the yield of photoproton reactions on the heavy titanium isotopes ^{49,50}Ti.

DOI: 10.1134/S106377881502009X

1. INTRODUCTION

Photon–nucleus interaction at energies ranging from values in excess of the nucleon-separation energy to approximately 40 MeV is determined by the excitation of a fundamental collective nuclear mode in the form of a giant dipole resonance. The properties of the giant dipole resonance—first of all, its shape and branching ratios for its decay through various channels—are sensitive to individual features of nuclei like the mass number A and the proton-to-neutron number ratio Z/N. By studying the photodisintegration of nuclei, one can therefore trace the relationship between individual features of a nucleus in the ground state and their counterparts in the energy region corresponding to the excitation of the giant dipole resonance and obtain deeper insight into physics behind this relationship. The state-of-the-art technique in photonuclear experiments makes it possible to follow the changes in the properties of the giant dipole resonance in response to successive changes in the number of protons or neutrons in target nuclei. Nuclide chains in a natural mixture of isotopes are the most convenient objects for such investigations.

The photon-activation method is the most appropriate for such investigations. In experiments of this type, a natural mixture of isotopes is irradiated with bremsstrahlung gamma radiation from an electron accelerator of energy that exceeds the energy corresponding to the maximum of the giant dipole resonance. In targets, different (mostly photonucleon) photonuclear reactions proceed in different isotopes. In some cases, nuclei produced in these reactions are beta-active and undergo respective decay, after which final-state nuclei arise in low-lying excited states whose spectrum is well known. This opens the possibility for selecting specific photodisintegration channels by means of high-resolution gamma spectroscopy and for measuring the yield of the respective reaction. A determination of the yields of different reactions on different isotopes under identical experimental conditions is an important advantage of this procedure. This permits reliably revealing effects associated with the change in the basic features of the giant dipole resonance in response to the successive change in number of neutrons in the chain of nuclei in a natural mixture of target isotopes.

In the present study, the photon-activation method is used to determine the yields of the photonucleon reactions on nuclei of titanium in its natural isotopic mixture. A natural mixture of titanium isotopes contains five isotopes (we gave parenthetically their concentrations in percent): ^{46}Ti (8.0), ^{47}Ti (7.3), ^{48}Ti (73.8), ^{49}Ti (5.5), and ^{50}Ti (5.4). The experimental yields are compared with the results of theoretical calculations based on the the widely used TALYS code [1] and on the combined photonuclear-reaction model (CPNRM) developed at the Skobeltsyn Institute of Nuclear Physics (Moscow State Univer-

[1)]Moscow State University, Moscow, 119991 Russia.
[2)]Institute for Nuclear Research, Russian Academy of Sciences, pr. Shestidesyatiletiya Oktyabrya 7a, Moscow, 117312 Russia.
[3)]Skobeltsyn Institute of Nuclear Physics, Moscow State University, Moscow, 119991 Russia.
[*]E-mail: kuznets@depni.sinp.msu.ru

Table 1. Results of earlier investigations of the photodisintegration of titanium isotopes

Target	Reaction	E_m, MeV	σ_m, mb	$E_{\max}$, MeV	σ_{int}, MeV mb	References
Ti (nat)	$^{46}\text{Ti}(\gamma,n)+0.91^{47}\text{Ti}(\gamma,2n)+1.36^{46}\text{Ti}(\gamma,pn)$	15.8 18.0	24.1 23.9	25	194 ± 40	[7]
Ti (nat)	$^{46}\text{Ti}(\gamma,n)+0.91^{47}\text{Ti}(\gamma,2n)$	20.5	31	31	260 ± 34	[3]
Ti (nat)	$^{46}\text{Ti}(\gamma,np)$	28.5	5	31	4.4–8.8	[3]
^{46}Ti (81.2)	$(\gamma,p)+(\gamma,np)+2(\gamma,2p)$ [from $(e,e'p)$]	20.3	37	25	216	[4]
Ti (nat)	$^{47}\text{Ti}(\gamma,p)+10.1^{48}\text{Ti}(\gamma,np)$	21	23	31	246 ± 38	[3]
Ti (nat)	$^{48}\text{Ti}(\gamma,p)+0.075^{49}\text{Ti}(\gamma,np)$	22.5	28.5	31	217 ± 32	[3]
^{48}Ti (99.3)	$(\gamma,p)+(\gamma,np)+2(\gamma,2p)$ [from $(e,e'p)$]	20.5 24	32 26	27	238	[6, 9]
^{48}Ti (99.3)	$(\gamma,n)+(\gamma,np)+2(\gamma,2n)$	16.1 17.5 19.5	48.6 46.4 43.6	27	398 ± 25	[9]
Ti (nat)	$^{49}\text{Ti}(\gamma,p)+0.98^{50}\text{Ti}(\gamma,np)$	21.5	11	31	82 ± 13	[3]
^{50}Ti (68.1)	$(\gamma,n)+(\gamma,np)+2(\gamma,2n)$	18.3	82	26.3	473	[8]
^{50}Ti (68.1)	$(\gamma,p)+(\gamma,np)+2(\gamma,2p)$ [from $(e,e'p)$]	22.6	17.5	26.3	96	[5, 8]
Ti (nat)	$^{50}\text{Ti}(\gamma,p)$	22.2	15	31	113 ± 32	[3]

sity) [2]. Conclusions concerning the predictive power of either model will be drawn.

2. INVESTIGATIONS OF THE PHOTODISINTEGRATION OF TITANIUM ISOTOPES

Earlier experimental investigations into the photodisintegration of titanium isotopes are presented in [3–9]. Some results of these investigations are given in Table 1. In all of the studies listed in Table 1, the energy dependence of the cross sections was determined for the corresponding photodisintegration reaction. In the "target" column, we give parenthetically the isotope content in the target: the label "nat" denotes a natural mixture of isotopes, while a value in parentheses is the concentration (in percent) of the respective isotope in an enriched target. In front of each reaction in the "Reaction" column, we give the numerical factor with which this reaction appears in the cross section formed by several reactions. Further, E_m represents the energies of the dominant maxima in the cross section, σ_m stands for the cross sections at the respective maxima, $E_{\max}$ is the maximum photon energy to which we have studied the reaction cross section, and σ_{int} is the integrated reaction cross section.

The experiments that were reported in [4–6, 8] and whose results are presented in Table 1 were performed with enriched titanium isotopes. A comparatively low maximum photon energy of 25 to 27 MeV, which does not cover the whole region of the giant dipole resonance, is a common drawback of all of these experiments. Above this boundary, we have a high-energy segment of the giant dipole resonance (its fraction in the integrated cross section amounts to about 40%), and, what is of importance, the high-isospin branch of the giant dipole resonance occupies this segment.

The differential cross sections for the process combining three reactions, $(\gamma,p)+(\gamma,np)+2(\gamma,2p)$, at the proton-detection angle of 90° were obtained from the investigations that were performed in the $(e,e'p)$ experiments reported in [4–6] and which were devoted to exploring the photoproton channel of giant-dipole-resonance decay in the titanium isotopes ^{46,48,50}Ti. The virtual-photon technique was applied. Because of the difficulties in processing experimental data, the use of this technique is inferior, however, to the use of real photons. Moreover, the total cross sections could be obtained from the differential cross sections only under the assumption that the angular distributions of protons are isotropic. The degree of enrichment of the target isotope also contributes to the uncertainty in the experimental results. By way of example, we indicate that, in the case of ^{50}Ti, for which the photoproton channel carries important information about the role of the isospin in the formation and decay of the giant dipole resonance in titanium isotopes, the enrichment did not exceed 70%. With allowance for all of the foregoing, the problem of exploring the photoproton channel of giant-dipole-resonance decay in titanium isotopes by the modern photon-activation procedure

Table 2. Features of the isospin splitting of the giant dipole resonance that were obtained in [12] for even–even titanium isotopes along with their counterparts found in [10, 11] by means of the standard approach

Isotope	$E_> - E_<$, MeV		$S_>/S_<$	
	[10, 11]	[12]	[10, 11]	[12]
^{46}Ti	2.6	3.28	0.79	0.25
^{48}Ti	3.8	7.82	0.35	0.12
^{50}Ti	4.8	7.15	0.20	0.15

Table 3. Stable titanium isotopes, their concentration η (in percent) in a natural mixture, and thresholds $E_{\gamma\text{thr}}$ for the quoted reactions on the respective isotopes

Isotope; concentration η (in percent) in natural mixture, %	Reaction thresholds $E_{\gamma\text{thr}}$, MeV					
	(γ, n)	(γ, p)	(γ, np)	$(\gamma, 2n)$	$(\gamma, 2p)$	$(\gamma, 3n)$
^{46}Ti; 8.0	13.2	10.3	21.7	22.7	17.2	39.0
^{47}Ti; 7.3	8.9	10.5	19.2	22.1	20.8	31.6
^{48}Ti; 73.8	11.6	11.4	22.1	20.5	19.9	33.7
^{49}Ti; 5.5	8.2	11.4	19.6	19.8	22.8	28.7
^{50}Ti; 5.4	10.9	12.2	22.3	19.1	21.8	30.7

over a broad region of photon-beam energies has still remained urgent.

The results obtained in [3, 4, 7–9] by experimentally studying the giant dipole resonance for the even–even stable titanium isotopes ^{46,48,50}Ti were compared with the results of theoretical calculations for the photodisintegration process. The calculations were performed by using nearly the same scheme. For the giant dipole resonance, use was made of a smoothed (structureless) sum of experimental photonucleon cross sections. Further, we consider the statistical mechanism of decay of the giant dipole resonance and take into account its isospin splitting. The properties of isospin splitting were calculated with the aid of the isospin Clebsch–Gordan coefficients and standard formulas for the concept of isospin splitting of the giant dipole resonance [10, 11]; that is,

$$\Delta E = E_> - E_< = \frac{60}{A}(T_0 + 1)\,[\text{MeV}], \qquad (1)$$

$$\frac{S_>}{S_<} = \frac{\int \sigma_>(E)/EdE}{\int \sigma_<(E)/EdE} = \frac{1}{T_0}\frac{1 - 1.5T_0A^{-2/3}}{1 + 1.5A^{-2/3}}, \qquad (2)$$

where $T_0 = \left|\frac{N-Z}{2}\right|$ is the ground-state isospin of the nucleus being considered; $E_>$ and $E_<$ are the mean energies of the giant-dipole-resonance components whose isospins are $T_< = T_0$ and $T_> = T_0 + 1$, respectively; and $\sigma_<$ and $\sigma_>$ are the cross sections for the corresponding isospin components. It was shown that, without allowance for the concept of isospin splitting of the giant dipole resonance, the ratio of the photoproton and photoneutron cross sections and the energy shift between them could not be explained.

The microscopic calculations of the giant dipole resonance for even–even titanium isotopes were performed in [12]. Use was made there of the *particle–final-nucleus state* (PFNS) version of the particle–hole formalism of the shell model. The energy distribution of hole configurations was taken into account, this distribution being extracted from spectroscopic data on direct (p, d) reactions. A rather complicated structure of the giant dipole resonance and a pronounced isospin splitting were obtained, the features of this splitting being given in Table 2, along with the predictions of the standard model from [10, 11]. Also, the photoneutron form factors were calculated under the assumption that the giant dipole resonance undergoes only semidirect decay, and the results were found to reproduce the shape of the experimental photoneutron cross sections.

The method of calculations in question also makes it possible to estimate the scale of the configuration splitting of the giant dipole resonance in titanium isotopes. It is not large but grows with the neutron excess, reaching the value of 5.0 MeV for the isotope ^{50}Ti.

All of the aforementioned calculations demonstrate the importance of the isospin splitting of the giant dipole resonance in even–even titanium isotopes and the need for further testing this concept over the whole chain of stable titanium isotopes both in experiments and in new theoretical calculations that would take into account all basic factors affecting the formation and decay of the giant dipole resonance.

3. EXPERIMENTAL PROCEDURE AND RESULTS

The photon-activation method used in this study was described in detail elsewhere [13–16]. Our experiment was performed at a pulsed racetrack microtron [17] by using an extracted electron beam of energy $E_e = 55$ MeV. The electron beam bombarded a tungsten radiator 2.1 mm thick. A metallic target in the form of a titanium foil 0.06 mm thick having a natural isotopic composition was irradiated with bremsstrahlung photons produced in the radiator. The target placed on the beam axis adjacent to the radiator overlapped almost completely the

^{43}Ti 509 ms β^+	^{44}Ti 63 yr EC	^{45}Ti 184.8 min β^+	**^{46}Ti** **8.0%**	**^{47}Ti** **7.3%**	**^{48}Ti** **73.8%**	**^{49}Ti** **5.5%**	**^{50}Ti** **5.4%**	^{51}Ti 5.76 min β^-
^{42}Sc 0.68 s, 61 s β^+	^{43}Sc 3.891 h β^+	^{44}Sc 3.9 h, 59 h β^+, IT	**^{45}Sc** **100%**	^{46}Sc 83.8 day, 19 s β^-, IT	^{47}Sc 3.3492 day β^-	^{48}Sc 43.67 h β^-	^{49}Sc 57.2 min β^-	^{50}Sc 102.5 s β^-

Fig. 1. Part of the $N-Z$ diagram of nuclei in the vicinity of stable titanium isotopes. The stable titanium and scandium isotopes are shaded in black (the concentrations of stable isotopes in percent in the natural mixture are given). Gray and white colors are used for, respectively, neutron-deficient and neutron-rich radioisotopes. The half-lives and decay modes are indicated for the radioisotopes (including their isomers).

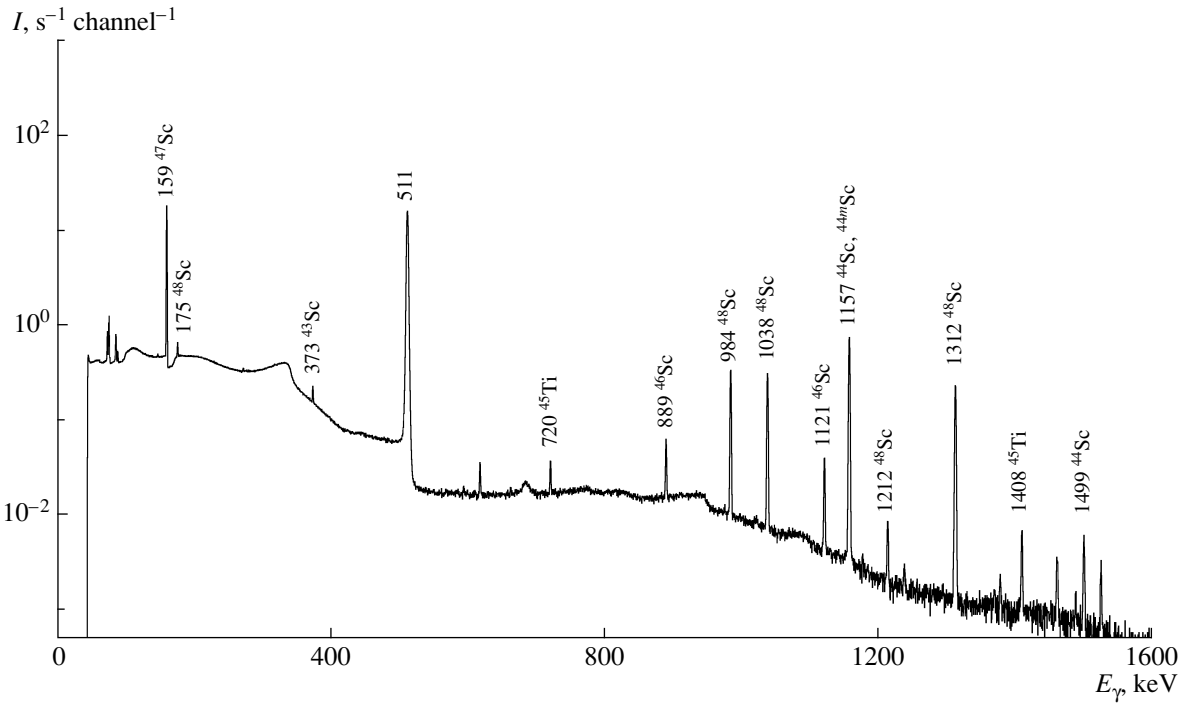

Fig. 2. Photon spectrum $I(E_\gamma)$ measured with the aid of a HPGe spectrometer for an irradiated titanium sample. The energies of the γ lines (in keV units) are indicated on the peaks along with the corresponding radioisotopes of titanium and scandium.

bremsstrahlung-photon beam. In the irradiation process, the average electron-beam current was 45.4 nA. The irradiation time was 1 h. After the irradiation, the target was transported to a photon spectrometer from high-purity germanium (HPGe spectrometer). The distance between the irradiated target and the entrance window of the HPGe spectrometer was 5 cm. Measurement of the residual activity of the irradiated target began in 19 min after the termination of the irradiation and lasted for 9 h.

Figure 1 shows part of the $N-Z$ diagram for nuclei in the vicinity of stable titanium isotopes and final-state nuclei produced in possible photonucleon reactions on them.

Table 3 gives thresholds for various photonuclear reactions that could be induced in a titanium target of natural isotopic composition by the bremsstrahlung beam used.

For various radioisotopes, the activities generated in a titanium target upon irradiation and reduced to the time of termination of this irradiation were calculated on the basis of an analysis of the spectra measured with the aid of the HPGe spectrometer by using characteristic gamma lines of each radioisotope with allowance for the quantum yield η of these lines. The detection efficiency of the HPGe spectrometer for photons of various energy was calibrated on the basis of measurements of activities of reference radioactive

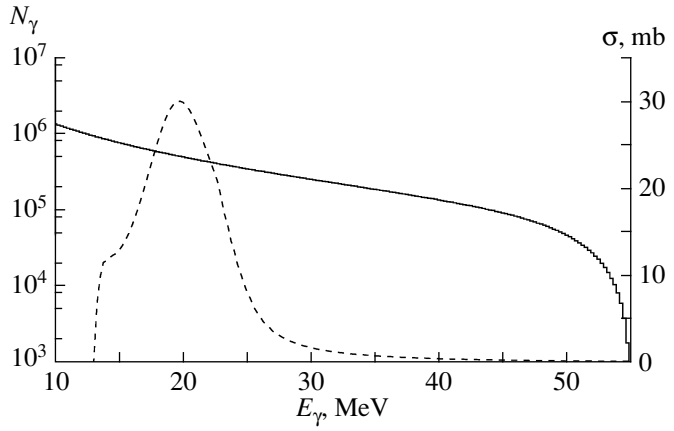

Fig. 3. Spectrum of bremsstrahlung photons from the tungsten radiator 2.1 mm thick at $E_e = 55$ MeV (solid curve) according to calculations based on the GEANT4 code [18] and cross section for the reaction $^{46}\mathrm{Ti}(\gamma, n)^{45}\mathrm{Ti}$ (dashed curve) according to calculations based on the TALYS code [1].

sources and also on the basis of a simulation according to the GEANT4 code [18].

Figure 2 shows one of the measured photon spectra for the decay of radioisotopes produced in an irradiated titanium target.

The observed peaks in the spectrum for radionuclides produced in photonuclear reactions accompanied by the emission of nucleons were identified and compared with known γ lines of final nuclei. In Table 4, we list the energies of the most intense gamma lines of the radioisotopes ^{45}Ti, ^{46}Sc, ^{47}Sc, ^{48}Sc, and ^{49}Sc produced in the titanium targets used. By using these lines, we identified photonuclear reactions that led to the production of the respective radioisotope and determined their yield. A large yield of the radioisotope ^{47}Sc in relation to other radioisotopes was due to a high concentration of the isotope ^{48}Ti in a natural mixture of titanium isotopes.

From experiments involving photon bremsstrahlung, one can obtain the photonuclear-reaction yield $Y(E_e)$, which is the convolution of the photonuclear-reaction cross section $\sigma(E_\gamma)$ and the bremsstrahlung-photon spectrum $\Phi(E_\gamma, E_e)$; that is,

$$Y(E_e) = \int_{E_{\mathrm{thr}}}^{E_e} \Phi(E_\gamma, E_e)\sigma(E_\gamma)dE_\gamma, \qquad (3)$$

where E_e is the kinetic energy of electrons incident to the radiator, E_γ is the energy of bremsstrahlung photons emitted from the radiator, and E_{thr} is the threshold for the photonuclear reaction under consideration. At the present time, there are computer codes (GEANT4 [18], for example) that allow one to calculate bremsstrahlung-photon spectra (see Fig. 3) to a high degree of precision for various experimental conditions.

The experimental results are presented in Table 4. We have listed there the observed photonucleon reactions, the half-lives of product radioisotopes, the peaks in the gamma spectrum that were used to identify a specific reaction and to calculate its yield, and the quantum output of each gamma line. The yield of reactions leading to the production of the radioisotope ^{45}Ti was taken to be unity. The contributions of individual titanium isotopes to these yields were proportional to their concentration (in percent). The yields with allowance for the concentrations of the isotopes in question are given below in Table 5 (see next section).

4. DISCUSSION OF THE RESULTS

In order to analyze the experimental results that we obtained we have performed calculations on the basis of the TALYS code [1] and on the basis of the combined photonuclear-reaction model proposed in [2]. The combined photonuclear-reaction model relies on a semimicroscopic description of the excitation of collective resonance states and employs the random-phase approximation (RPA). It takes into account the giant dipole resonance, together with its overtone, and the quadrupole resonance, as well as the quasideuteron photon-absorption mechanism. The most important effects that determine the structure of the giant dipole resonance, its deformation splitting, and its isospin splitting are reflected in the model at the microscopic level. In the TALYS code, use is made of the data on photoabsorption cross sections from the RIPL-3 (Reference Input Parameter Library) experimental database of evaluated data [19]. A combination of the Hauser–Feshbach evaporation mechanism and the preequilibrium exciton mechanism of compound-nucleus decay accompanied by

Table 4. Production of radioisotopes in photonuclear reactions on the natural titanium ($T_{1/2}$ is the half-life of a radioisotope, E_γ stands for photon energies used to identify radioisotopes, η_γ is the quantum output of photons, and Y_{rel} is the radioisotope yield normalized to the ^{45}Ti yield)

Radioisotope	Dominant reactions	$T_{1/2}$	E_γ, keV	η_γ	Y_{rel}
^{45}Ti	$^{46}\text{Ti}(\gamma, n)^{45}\text{Ti}$	184.8 min	720.2 1408.6	0.00154 0.00085	1.0 ± 0.1
^{46}Sc	$^{47}\text{Ti}(\gamma, p)^{46}\text{Sc} +$ $+ \, ^{48}\text{Ti}(\gamma, pn)^{46}\text{Sc}$	83.79 day	889.3 1200.5	0.99984 0.99987	0.95 ± 0.10
^{47}Sc	$^{48}\text{Ti}(\gamma, p)^{47}\text{Sc}$	3.3492 day	159.4	0.683	3.14 ± 0.31
^{48}Sc	$^{49}\text{Ti}(\gamma, p)^{48}\text{Sc}$	43.76 h	983.5 1037.6 1212.9 1312.1	1.001 0.976 0.0238 1.001	0.18 ± 0.02
^{49}Sc	$^{50}\text{Ti}(\gamma, p)^{49}\text{Sc}$	57.2 min	1622.6 1762.0	0.0001 0.0005	0.12 ± 0.03

Table 5. Ratios of the yields of photonuclear reactions on titanium isotopes to the ^{45}Ti yield according to the data of our present experiment and according to calculations based on the TALYS code and on the combined photonuclear-reaction model (CPNRM) [in the case of the yield of an isotope produced in two or three reactions, the number before the second (third) reaction takes into account the relative content of the corresponding isotope in the natural mixture of titanium isotopes]

Isotope	Reaction	Relative yield		
		TALYS	CMPhR	Present study
^{45}Ti	$^{46}\text{Ti}(\gamma, n) + 0.91^{47}\text{Ti}(\gamma, 2n)$	1.0	1.0	1.0 ± 0.1
^{45}Sc	$^{46}\text{Ti}(\gamma, p) + 0.91^{47}\text{Ti}(\gamma, pn) + 9.23^{48}\text{Ti}(\gamma, p2n)$	0.239	0.314	
^{46}Sc	$^{47}\text{Ti}(\gamma, p) + 10.1^{48}\text{Ti}(\gamma, pn)$	0.158	0.229	0.179 ± 0.02
^{47}Sc	$^{48}\text{Ti}(\gamma, p)$	0.615	1.223	0.651 ± 0.06
^{48}Sc	$^{49}\text{Ti}(\gamma, p) + 0.98^{50}\text{Ti}(\gamma, pn)$	0.119	0.320	0.257 ± 0.028
^{49}Sc	$^{50}\text{Ti}(\gamma, p)$	0.053	0.374	0.340 ± 0.085

the emission of nucleons and photons is applied in both models.

In order to perform a comparison with the results of these calculations, it was necessary to choose the most convenient representation of the experimental data. In the representation that we choose, the quantities under comparison are given in Table 5. First, the relative concentration of the respective isotope in a natural mixture of titanium isotopes was taken into account in all yields of radionuclides, both experimental and theoretical, that were produced in two or three reactions. For example, the reaction form $^{47}\text{Ti}(\gamma, p) + 10.1^{48}\text{Ti}(\gamma, pn)$ reflects the fact that the concentration of the isotope ^{48}Ti (73.8%) in a natural mixture is 10.1 times as high as the concentration of the isotope ^{47}Ti (7.3%). Second, all photoproton yields were normalized to the yield of the photoneutron reaction $^{46}\text{Ti}(\gamma, n) + 0.91^{47}\text{Ti}(\gamma, 2n)$, whereby it is shown how the photoproton yield changes upon going over from one isotope to another.

From Table 5, one can see that the calculations of the photoproton-reaction yields both on the basis

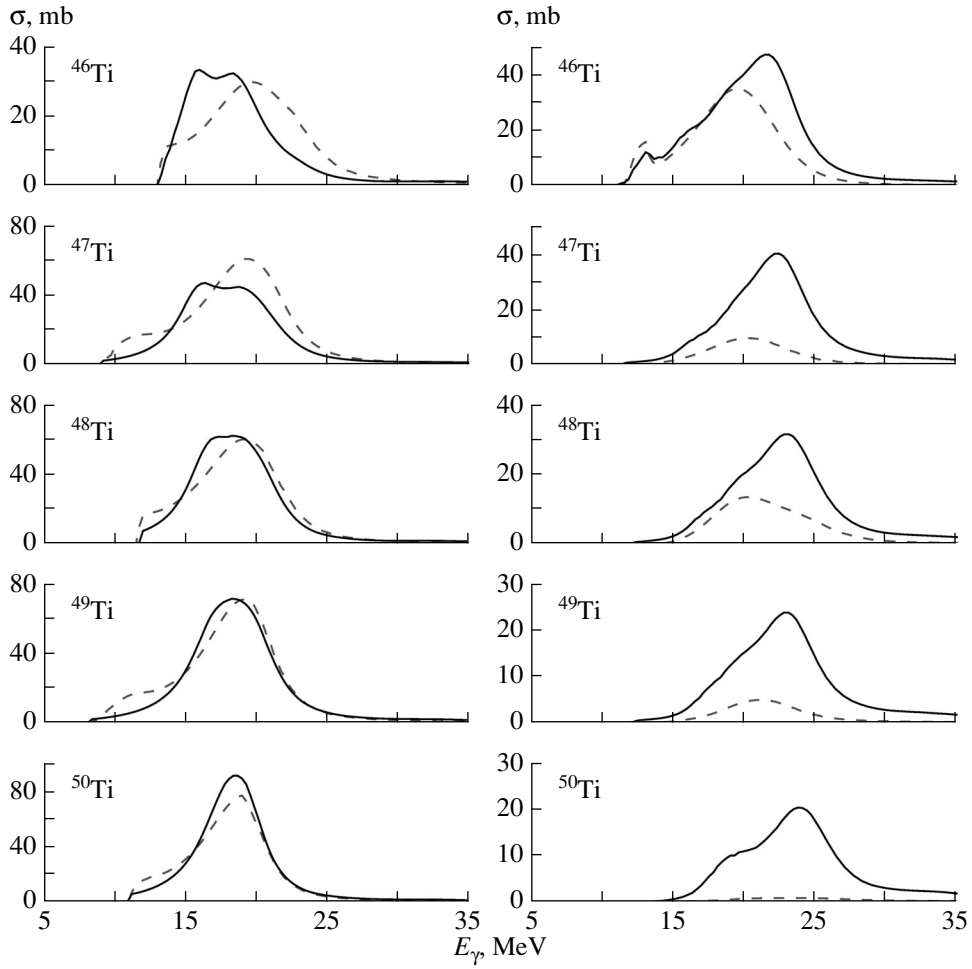

Fig. 4. Cross sections for (left-hand column of panels) (γ, n) and (right-hand column of panels) (γ, p) reactions according to calculations based on the (dashed curves) TALYS code and (solid curves) combined photonuclear-reaction model.

of the TALYS code and on the basis of the combined photonuclear-reaction model reproduce satisfactorily experimental data for three light stable titanium isotopes—^{46}Ti, ^{47}Ti, and ^{48}Ti. At the same time, the TALYS code does not reproduce the photoproton yields for two heavy stable titanium isotopes—^{49}Ti and ^{50}Ti. The photoproton yield calculated on the basis of the TALYS code is less than its experimental counterpart by a factor greater than two for ^{49}Ti and by a factor greater than six for ^{50}Ti. In contrast to the TALYS calculations, the calculations based on the combined photonuclear-reaction model for ^{49}Ti and ^{50}Ti yield results that agree with respective experimental data. The reason behind this discrepancy in the description of experimental data is that, in dealing with photoproton reactions, the TALYS code disregards the isospin structure of the giant dipole resonance, but, without taking this structure into account, it is impossible to describe correctly the branching ratios for the decay of the giant dipole resonance through channels involving the emission of protons and neutrons. It is precisely the inclusion of the isospin structure the giant dipole resonance that is the feature of importance distinguishing the combined photonuclear-reaction model, where it is present, from the TALYS code, where it is absent. In contrast to the $T_<$ isospin component of the giant dipole resonance, its $T_>$ component may decay through the neutron channel only to high-lying energy levels of the final nucleus because of isospin conservation, and this leads to a predominant emission of protons from this state, the effect in question being especially strong for isotopes featuring a relatively high neutron excess.

The potential of the TALYS code and the potential of the combined photonuclear-reaction model for describing the photodisintegration of titanium isotopes are illustrated by Figs. 4 and 5. In Fig. 4, the cross sections obtained for the (γ, n) and (γ, p)

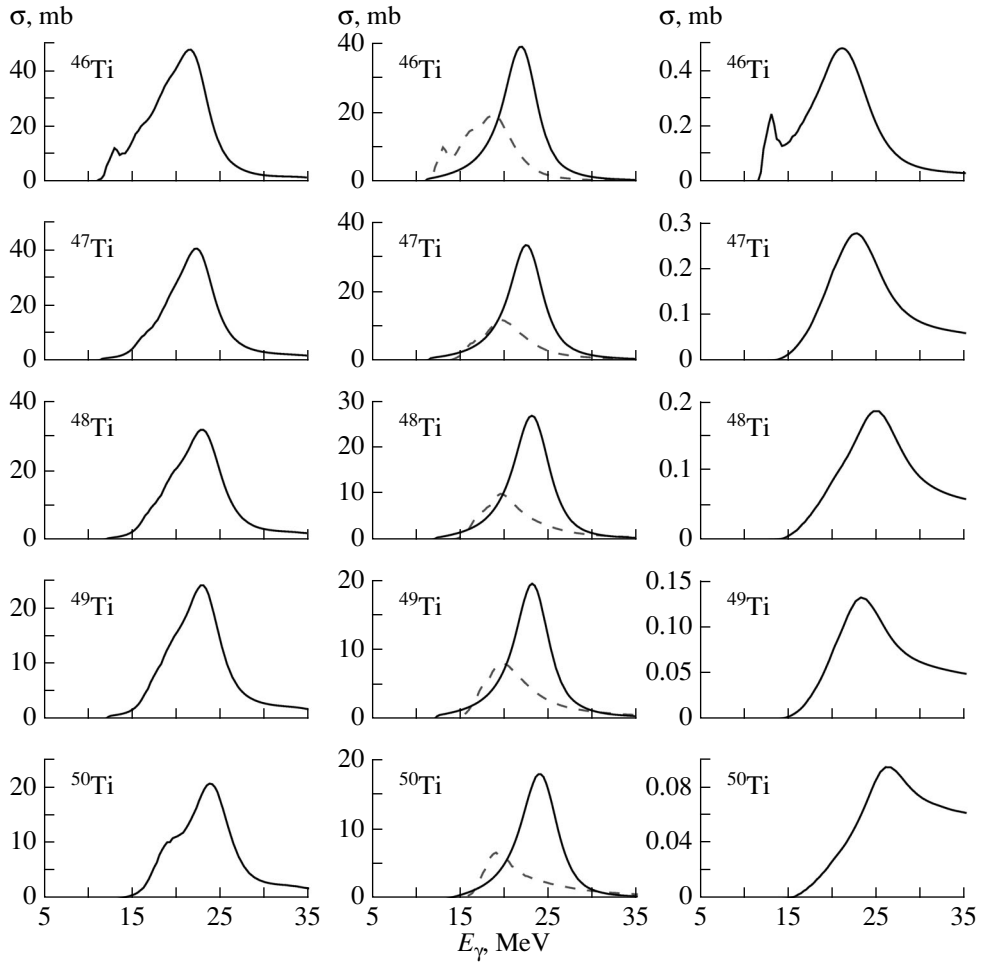

Fig. 5. Cross sections for (γ, p) reaction on titanium isotopes (left-hand column of panels) results of calculations based on the combined photonuclear-reaction model, (middle-column of panels) isospin cross-section components represented by the dashed curves for $T_<$ and the solid curves for $T_>$, and (right-hand column of panels) quasideuteron component of the (γ, p) cross section.

reactions on the basis of the TALYS code and the combined photonuclear-reaction model are compared for stable titanium isotopes. Figure 5 shows how the isospin components, which form the photoproton cross sections for titanium isotopes, look in the calculations based on the combined photonuclear-reaction model. Figures 4 and 5 clearly demonstrate the difference in the description of the photoproton channel of giant-dipole-resonance decay in titanium isotopes on the basis of the TALYS code and on the basis of the combined photonuclear-reaction model. Obviously, this difference is due to the inclusion of the isospin structure of the giant dipole resonance in the combined photonuclear-reaction model—that is, to the presence of two isospin components of the giant dipole resonance, that of isospin $T_< = T_0 = \left|\frac{N-Z}{2}\right|$ and that of isospin $T_> = T_0 + 1$. The relative contribution of the $T_>$ component, which is disregarded in the TALYS code and which is taken into account in the combined photonuclear-reaction model, grows with increasing neutron excess and explains the observed value of the photoproton cross sections for the isotopes ^{49}Ti and ^{50}Ti.

Our experimental and theoretical investigations of the photodisintegration of titanium isotopes make it possible to determine not only the yields of photoproton reactions for these isotopes but also the respective integrated cross sections. A transitions from the yields to the integrated cross sections is possible owing to small changes in the number of photons in the bremsstrahlung spectrum at energies in the region around the maximum of the giant dipole resonance. Their number in the bremsstrahlung spectrum whose endpoint energy is $E_e = 55$ MeV changes within 15 to 20%. This permits going over, to approximately the same degree of precision, from the ratio of the reaction yields to the ratio of the integrated cross sections for

Table 6. Integrated cross sections for photonucleon reactions on titanium isotopes at energies of up to 55 MeV according to calculations based on the TALYS code and on the combined photonuclear-reactions model along with their counterparts obtained in our experiment

Reaction	Integrated cross section, MeV mb		
	TALYS	CPNRM	Present work
$^{46}\mathrm{Ti}(\gamma,n)^{45}\mathrm{Ti} + ^{47}\mathrm{Ti}(\gamma,2n)^{45}\mathrm{Ti}$	329	278	280 ± 50
$^{46}\mathrm{Ti}(\gamma,p)^{45}\mathrm{Sc} + ^{47}\mathrm{Ti}(\gamma,pn)^{45}\mathrm{Sc} + ^{48}\mathrm{Ti}(\gamma,p2n)^{45}\mathrm{Sc}$	417	525	
$^{47}\mathrm{Ti}(\gamma,p)^{46}\mathrm{Sc} + ^{48}\mathrm{Ti}(\gamma,pn)^{46}\mathrm{Sc}$	128	227	178 ± 33
$^{48}\mathrm{Ti}(\gamma,p)^{47}\mathrm{Sc}$	109	204	110 ± 19
$^{49}\mathrm{Ti}(\gamma,p)^{48}\mathrm{Sc} + ^{50}\mathrm{Ti}(\gamma,pn)^{48}\mathrm{Sc}$	56.8	125	101 ± 19
$^{50}\mathrm{Ti}(\gamma,p)^{49}\mathrm{Sc}$	12.7	74.8	68.5 ± 20

the same reactions; that is,

$$\frac{Y_1(E_e)}{Y_2(E_e)} = \frac{\int\limits_{E_{\mathrm{thr}}}^{E_e} \Phi(E_\gamma, E_e)\sigma_1(E_\gamma)dE_\gamma}{\int\limits_{E_{\mathrm{thr}}}^{E_e} \Phi(E_\gamma, E_e)\sigma_2(E_\gamma)dE_\gamma} \quad (4)$$

$$\approx \frac{\int\limits_{E_{\mathrm{thr}}}^{E_e} \sigma_1(E_\gamma)dE_\gamma}{\int\limits_{E_{\mathrm{thr}}}^{E_e} \sigma_2(E_\gamma)dE_\gamma} \approx \frac{\sigma_{1\mathrm{int}}}{\sigma_{2\mathrm{int}}}.$$

The results of estimating the integrated cross sections and of comparing them with the theoretical calculations are given in Table 6.

On the basis of Eq. (4), the integrated photoproton-reaction cross section $\sigma^{\mathrm{int}}_{\mathrm{expt.}}$ was calculated with the aid of the relation

$$\sigma^{\mathrm{int}}_{\mathrm{expt.}} = \sigma^{\mathrm{int}}_{\mathrm{CPhRM}} \frac{Y_{\mathrm{expt.}}(E_e)}{Y_{\mathrm{CPhRM}}(E_e)}, \quad (5)$$

where the yield $Y_{\mathrm{CPhRM}}(E_e)$ and the integrated cross section $\sigma^{\mathrm{int}}_{\mathrm{CPhRM}}$ for the reaction to which we normalized our cross sections were set the corresponding values calculated on the basis of the combined photonuclear-reaction model (CPNRM).

As was mentioned above, the error in the integrated cross sections is determined by the bremsstrahlung spectrum and the distinction between the actual shape of the cross section and its calculated counterpart. On the basis of a comparison with available experimental data, we estimate the error of expression (5) at 15%.

The quasideuteron-photodisintegration mechanism [20–22] is known to play an ever increasing role in the giant-dipole-resonance region and above it. This mechanism competes with the giant dipole resonance within its high-energy section. Since the endpoint energy of of the bremsstrahlung spectrum was 55 MeV in our experiment, it was necessary to assess the scale of the quasideuteron-photodisintegration contribution to the yields that we obtained. Within the combined photonuclear-reaction model, the quasideuteron-component contribution is calculated on the basis of the approximate formula from [22]. For all stable titanium isotopes, Fig. 5 gives the quasideuteron components of the cross sections up to the energy of 35 MeV. The results of the calculations reveal that the contribution of the quasideuteron photodisintegration mechanism to the formation of the photonucleon yields on titanium isotopes is negligible.

5. CONCLUSIONS

The photodisintegration of titanium isotopes in the giant-dipole-resonance region has been studied with the aid of the photon-activation method. Bremsstrahlung photons whose spectrum has the endpoint energy of 55 MeV has been used. The yields and integrated cross sections for the photoproton reactions on the isotopes $^{47,48,49,50}\mathrm{Ti}$ have been obtained. The experimental results have been compared with their counterparts calculated on the basis of the TALYS code and the combined photonuclear-reaction model. The combined photonuclear-reaction model describes satisfactorily the experimental data obtained here. The TALYS code leads to a severalfold underestimation of the yields for the heavy titanium isotopes $^{49,50}\mathrm{Ti}$. The reason is that, in contrast to the combined photonuclear-reaction model, the TALYS code disregards the isospin structure of the giant dipole resonance.

ACKNOWLEDGMENTS

We are grateful to N.G. Goncharova for providing us with the possibility of studying and employing the calculations of the photodisintegration of even–even stable titanium isotopes on the basis of the *particle–state of final nucleus* version that she developed within the particle–hole formalism of the shell model.

REFERENCES

1. A. J. Koning, S. Hilaire, and M. C. Duijvestijn, in *Proceedings of the International Conference on Nuclear Data for Science and Technology, Nice, France, Apr. 22–27, 2007,* Ed. by O. Bersillon, F. Crunsing, E. Bango, et al. (EDP Sciences, 2008), p. 211.
2. B. S. Ishkhanov and V. N. Orlin, Phys. At. Nucl. **74**, 19 (2011).
3. T. R. Sherwood and W. E. Turchinetz, Nucl. Phys. **29**, 292 (1962).
4. S. Oikawa and K. Shoda, Nucl. Phys. A **277**, 301 (1977).
5. M. N. Thompson et al., Res. Rep. Labor. Nucl. Sci., Tohoku Univ. **10**, 55 (1977).
6. J. Weise, et al., Res. Rep. Labor. Nucl. Sci., Tohoku Univ. **11**, 43 (1978).
7. R. E. Pywell and M. N. Thompson, Nucl. Phys. A **318**, 461 (1979).
8. R. E. Pywell, M. N. Thompson, and R. A. Hicks, Nucl. Phys. A **325**, 116 (1979).
9. R. Sutton, M. N. Thompson, M. Sugawara, et al., Nucl. Phys. A **339**, 125 (1980).
10. S. Fallieros and B. Goulard, Nucl. Phys. A **147**, 593 (1970).
11. R. Ö. Akyüz and S. Fallieros, Phys. Rev. Lett. **27**, 1016 (1971).
12. N. G. Goncharova and Yu. A. Skorodumina, Bull. Russ. Acad. Sci.: Phys. **76**, 1085 (2012).
13. S. S. Belyshev, L. Z. Dzhilavyan, A. N. Ermakov, et al., Moscow Univ. Phys. Bull. **67**, 246 (2012).
14. S. S. Belyshev, L. Z. Dzhilavyan, A. N. Ermakov, et al., Bull. Russ. Acad. Sci.: Phys. **77**, 480 (2013).
15. S. S. Belyshev, A. N. Ermakov, B. S. Ishkhanov, et al., Nucl. Instrum. Methods Phys. Res. A **745**, 133 (2014).
16. S. S. Belyshev, L. Z. Dzhilavyan, B. S. Ishkhanov, et al., Moscow Univ. Phys. Bull. **69**, 363 (2014).
17. A. I. Karev, A. N. Lebedev, V. G. Raevsky, et al., in *Proceedings of 22nd Russian Particle Accelerator Conference (RuPAC-2010)*, p. 316.
18. S. Agostinelli, J. Allison, K. Amako, et al., Nucl. Instrum. Methods Phys. Res. A **506**, 250 (2003).
19. R. Capote, M. Herman, P. Obložinský, et al., Nucl. Data Sheets **110**, 3107 (2009).
20. J. S. Levinger, Phys. Rev. **84**, 43 (1951).
21. J. S. Levinger, Phys. Lett. **82**, 181 (1979).
22. M. B. Chadwick, O. Obloinský, P. E. Hodgson, and G. Reffo, Phys. Rev. C **44**, 814 (1991).